

# Chapter 7

## Acceptance

### 7.1 Definition and calculation

Acceptance is a ratio of decays detected to decays present; it is an efficiency or probability for a physical state to satisfy requirements (some of them purely stochastic) that allow for a positive measurement to be made. In the context of this analysis, this physical event is a charm meson decay  $D \rightarrow xyz$  ( $x_F > 0$ ), where the two to three charged decay products are comprised of pions and at least one kaon. A “positive measurement” of such an event has many components.

First, the event must have been written to tape. This requirement entails two efficiencies,  $\epsilon_{live}$  and  $\epsilon_{trig}$ , the first being the detector livetime and the second being the efficiency for the event to pass a particular set of trigger requirements (labelled  $T$ ). As detailed in Section 8.1,  $\epsilon_{live}$  is included in the “live flux” component of the absolute cross-section calculation and therefore does not concern us here.<sup>1</sup>

Once an event is written to tape, detection depends on a multitude of interrelated factors: track reconstruction in the SMD and drift chambers; track matching between different regions of the spectrometer, allowing for momentum determination; Čerenkov identification of the kaon(s); and association of the tracks into primary and secondary vertices. Unlike the inherently binary selection criteria mentioned in

---

<sup>1</sup>Another factor which does not come into our definition of acceptance is beam-tagging efficiency. As shown in the calculation of Section 8.1, this efficiency either cancels out or is included in the flux calculation.

the previous paragraph, success in any of these processes is typically quantified in terms of one or more continuous variables.<sup>2</sup> For example, a track returned by the track-reconstruction algorithm (which takes as its inputs SMD and DC hits) will be associated with a value of the statistical measure  $\chi^2$ . Whether or not this track is deemed “good” (i.e., determines with sufficient precision the direction and location of a physical particle trajectory) will depend on whether its  $\chi^2$  falls above or below some cutoff. This and similar cutoffs (the so-called “analysis cuts”) are chosen to optimize particle detection, not by maximizing the overall efficiency but by maximizing the expected statistical significance of the measured physical parameters. This process is described in Section 5.5.

The average efficiency for a decay  $D \rightarrow xyz$  to pass all analysis cuts will be called  $\epsilon_{geom}$ , where the subscript gives the somewhat misleading impression that this efficiency is simply a function of the interrelated geometries of the particle decay and spectrometer. In fact,  $\epsilon_{geom}$  is a complex convolution of these geometrical dependencies with the efficiencies of each component of the detector, the details of the tracking and vertexing algorithms, and the values of the final analysis cuts. An analytic calculation of  $\epsilon_{geom}$  would be exceedingly difficult to perform, so we rely upon numerical methods, namely the Monte Carlo simulation of the experiment detailed in Chapter 4.

Acceptance is given by the following expression:

$$Acc(T, D \rightarrow xyz) = \epsilon_{geom}(D \rightarrow xyz) \epsilon_{trig}(T, D \rightarrow xyz) = \frac{\hat{N}_{obs}^{MC}(T, D \rightarrow xyz)}{N_{gen}^{MC}(D \rightarrow xyz)}, \quad (7.1)$$

where

$$\begin{aligned} \hat{N}_{obs}^{MC}(T, D \rightarrow xyz) &= \text{number of } \textit{weighted} \text{ MC } D\text{'s } (x_F > 0) \text{ observed through} \\ &\quad \text{invariant mass reconstruction of decay } D \rightarrow xyz, \text{ and} \\ N_{gen}^{MC}(D \rightarrow xyz) &= \text{number of generated MC } D\text{'s } (x_F > 0) \text{ decaying to } xyz. \end{aligned}$$

By weighting Monte Carlo events, we’re able to include efficiencies or corrections to the simulation without changing the code. The above definition of acceptance is also

---

<sup>2</sup>Ultimately, these continuous variables are derived statistically from sets of binary physical events, such as whether an SMD strip registered a hit or whether a phototube fired.

valid for the differential analysis, except that both  $\hat{N}_{obs}^{MC}$  and  $N_{gen}^{MC}$  are binned in  $x_F$  or  $p_T^2$  in order to determine acceptance as a function of these variables. In both differential and absolute cross-section analyses, the trigger efficiency is added through a weighting function. In the differential analysis, a Čerenkov efficiency correction is implemented. In the absolute analysis, corrections to the differential and lifetime distributions and drift chamber efficiencies are used. These weighting functions and factors are described in the following section.

## 7.2 Monte Carlo weighting

### 7.2.1 Trigger efficiency

As detailed in Section 6.2, different trigger combinations make up the data signals for each of E769's five beam particle types. The efficiency of each of these triggers has a transverse energy ( $E_T$ ) dependence which must be modelled in the MC in order to obtain the trigger efficiency  $\epsilon_{trig}$  for events containing a particular charm decay. This  $E_T$  dependence changes with run number, as both the trigger thresholds and trigger prescalers (which affect the relative fractions of each trigger in a given signal) were adjusted from time to time as the experiment progressed.

The  $E_T$  dependence of the efficiency of a particular combination of triggers over a certain run region is determined by measuring it directly using a set of about 1.2 million interaction triggers. The interaction trigger, once the effect of its (changing) prescaler has been removed, is taken to have an efficiency of 100% for charm. Rather than looking at calorimeter output directly (which would have to be modelled well in the MC), a measure of  $E_T$  called  $p_T(7, 15)$  is used. For a given event,  $p_T(7, 15)$  is the summed transverse momenta of all JCATSG<sup>3</sup> 7 and 15 charged tracks which pass a few loose cuts on track quality.

It has been determined that the  $p_T(7, 15)$  dependence of all E769 trigger efficiencies is well-parametrized by the following function:

---

<sup>3</sup>The variable JCATSG is defined in the footnote on pg. 36.

$$\epsilon_{trig}(p_T(7, 15)) = P_1 - \frac{P_2}{1 + \exp\left(\frac{p_T(7, 15) - P_3}{P_4}\right)} \quad (7.2)$$

$P_1$ - $P_4$  are parameters determined by a fit of efficiency versus  $p_T(7, 15)$ . For the trigger combinations/run regions used in this analysis, these parameters are listed in Table 7.1. The parameter  $P_1$  is the value to which the trigger efficiency function plateaus at high  $p_T(7, 15)$ ; we expect this to be 100% in the absence of prescaling.<sup>4</sup> For charm events, if the efficiency due to prescaling is removed, the remaining efficiencies due to the low and high- $E_T$  thresholds are approximately 75% (90%) and 10% (20%), respectively, during the negative (positive) running.

In Fig. 7.1, a fit to interaction trigger data is shown; the shape of the  $\epsilon_{trig}$  dependence on  $p_T(7, 15)$  seen here is typical. Since this dependence is non-linear, these parametrization functions are used to weight the MC on an event-by-event basis rather than to obtain trigger efficiencies from average values of  $p_T(7, 15)$ .

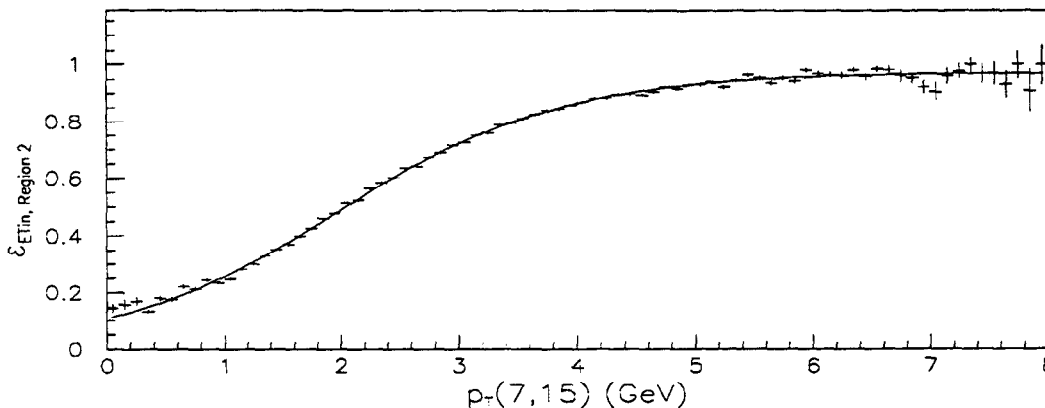


Figure 7.1: Trigger efficiency  $\epsilon_{ETin,Region2}$  vs.  $p_T(7, 15)$  (GeV).

Note that to model the average trigger efficiency in  $p$  beam data, a flux-weighted

<sup>4</sup>Trigger efficiency function parameters are determined from fits over the  $p_T(7, 15)$  range 0-8 GeV. The high- $E_T$  threshold was set above this range; therefore, for trigger combinations which include this requirement in their logic,  $\epsilon_{trig}$  does not turn over and reach a plateau value in a  $p_T(7, 15)$  range with a significant amount of data. In these cases,  $P_1$  should not be taken as a reliable estimate of the average inverse prescale setting.

Trigger(s)	Run region	$P_1^a$	$P_2$	$P_3$ (GeV)	$P_4$ (GeV)
ET $\pi$ +ETB	1	.519 $\pm$ .017	.50 $\pm$ .04	2.28 $\pm$ .07	1.08 $\pm$ .10
	2	.324 $\pm$ .013	.37 $\pm$ .02	2.90 $\pm$ .08	1.83 $\pm$ .12
ETin <sup>b</sup>	1	.954 $\pm$ .007	.88 $\pm$ .03	1.92 $\pm$ .05	.95 $\pm$ .04
	2	.973 $\pm$ .002	.976 $\pm$ .012	1.98 $\pm$ .02	.965 $\pm$ .014
ET $\pi$ +ETB+ETe	3	.160 $\pm$ .014	.163 $\pm$ .016	4.3 $\pm$ .2	1.52 $\pm$ .13
ETin	3	.9996 $\pm$ .0010	.770 $\pm$ .011	1.73 $\pm$ .03	.824 $\pm$ .011
ETin	4	.999 $\pm$ .005	.78 $\pm$ .05	1.71 $\pm$ .10	.83 $\pm$ .05

<sup>a</sup>In the differential cross-section analysis, weighting functions are multiplied by factors which lift their plateau values  $P_1$  up to 100% (if they're not there already). The normalization is corrected at the end of the analysis using results from the absolute cross-section analysis.

<sup>b</sup>The efficiency of the ETin requirement (defined in Section 3.5) is used to model the efficiency of ETK triggers, thereby eliminating the contribution of the DISC efficiency to the latter. This efficiency cancels out in the cross-section calculation, as described in Section 8.1.

Table 7.1: Trigger efficiency weighting function parameters.

sum of trigger efficiency functions, corresponding to the two independent trigger sets in this sample (ET $\pi$ +ETB+ETe in Region 3 and ETK in Region 4), is used. In the differential cross-section analysis, 210 and 250 GeV data is combined in the  $\pi^-$  and  $K^-$  samples; combined Region 1 and 2 trigger efficiency functions are therefore used to weight the MC.

## 7.2.2 Čerenkov efficiency

This analysis relies on identification of charged secondary kaons by the two threshold Čerenkov detectors in the E769 spectrometer. The efficiency for this identification  $\epsilon_{\check{C}(K)}$  is dependent upon the kaon momentum  $p_K$ . There is reason to doubt (on first principles), however, that the MC simulation of the Čerenkov counters is sophisticated enough to return a value for this efficiency accurate to within the precision afforded by MC statistics. A previous E769 graduate student therefore measured the dependence of  $\epsilon_{\check{C}(K)}$  on  $p_K$  directly using  $D^+ \rightarrow K\pi\pi$  data. In bins of  $p_K$ ,  $D^+$  signals were

obtained with and without a cut on the Čerenkov probability of the kaon. The ratio of these signals gives an average value of  $\epsilon_{\check{C}(K)}$  over a given range of  $p_K$ . The ratios of these data-determined efficiencies to their MC-determined counterparts provide a weighting function with which to correct the MC. A comparison of data and MC values of  $\epsilon_{\check{C}(K)}$  is shown in Fig. 7.2.

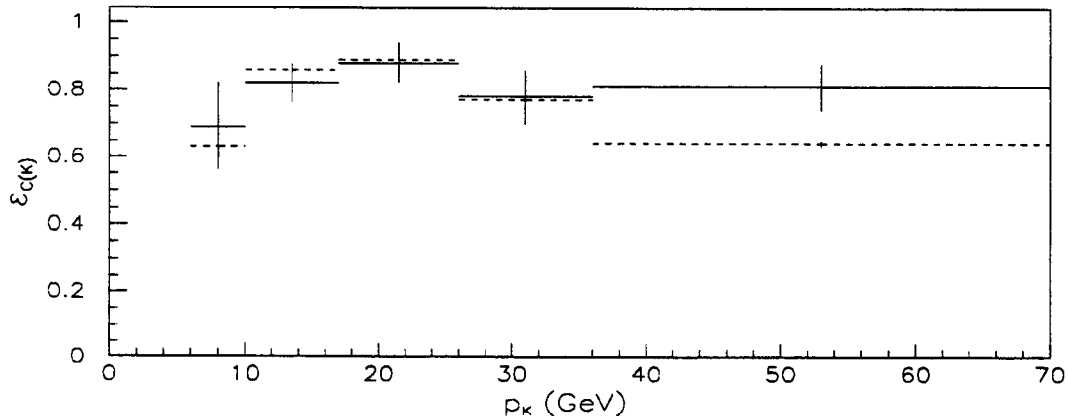


Figure 7.2: Čerenkov efficiency for  $K$  identification vs.  $p_K$  (GeV) from  $D^+ \rightarrow K\pi\pi$  data (solid) and MC (dashed).

As can be seen from the plot, on the basis of this data alone (which is statistics-limited), there is no compelling evidence that any correction is indicated. It was decided, therefore, that *no* Čerenkov correction to the MC would be made in the absolute cross-section analysis.<sup>5</sup> Due to the lingering uncertainty in  $\epsilon_{\check{C}(K)}$ , however, the precision of the aforementioned determination from data (which is the best information we have) is used as the measure of this contribution to the systematic uncertainty in the acceptance (see Section 8.2).

<sup>5</sup>At the time of this decision, the differential cross-section analysis had already been completed using the Čerenkov correction to weight the MC (once for each kaon among the decay products of a given mode) on an event-by-event basis. The effect of this weighting on the differential acceptances, however, is not significant.

### 7.2.3 Differential distributions

The acceptance for a particle  $D$  is a function of its momentum; due to the effective azimuthal symmetry of the spectrometer about the beam axis, it is reasonable to split this dependence into uncorrelated  $x_F$  and  $p_T^2$  parts. We rely upon the MC simulation of the  $D$  event in determining acceptance, both in the absolute and differential cross-section analyses. In the latter, however, data and MC signals are binned in  $x_F$  and  $p_T^2$  with sufficient fineness (given the observed variation of acceptance with the production variables) to ensure that results are insensitive to the  $x_F$  and  $p_T^2$  distributions generated for the  $D$  in the MC. This allows us to obtain differential cross-section results without making any assumptions about the distributions we expect (except perhaps that the real and MC-generated production distributions are qualitatively similar). These results in turn are used in the absolute cross-section analysis; MC events are weighted in both  $x_F$  and  $p_T^2$  in order to force the MC distributions in these variables to conform to measured results.

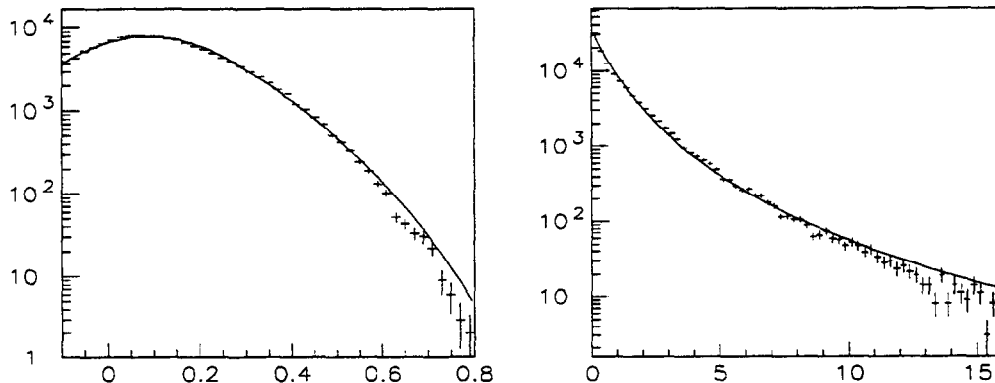


Figure 7.3: Number of generated  $D^+$  events vs.  $x_F$  (left) and  $p_T^2$  ( $\text{GeV}^2$ ) (right).

As described in detail in Section 9.3.3, for a given beam, combined  $D$  differential cross-sections are found to be consistent<sup>6</sup> with each of the distributions for  $D^+$ ,  $D^0$ , and  $D_s$ , taken separately. In addition, positive and negative-beam components of

<sup>6</sup>See Section 9.3.2 for a precise definition of “consistency” as it relates to two measured distributions.

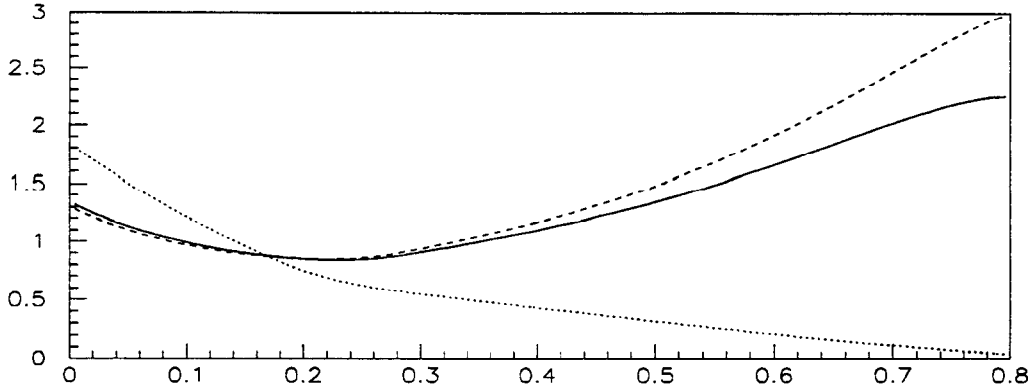


Figure 7.4:  $D^+$  production distribution correction vs.  $x_F$ , for  $\pi$  (solid),  $K$  (dashed), and  $p$  (dotted) beams.

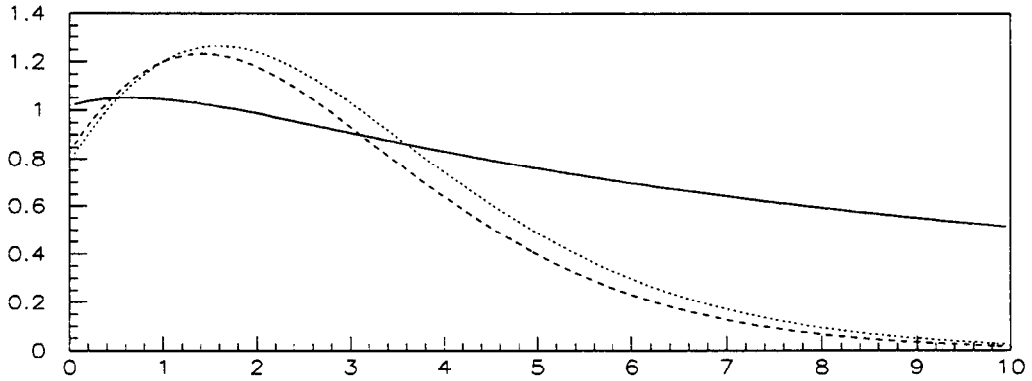


Figure 7.5:  $D^+$  production distribution correction vs.  $p_T^2$  ( $\text{GeV}^2$ ), for  $\pi$  (solid),  $K$  (dashed), and  $p$  (dotted) beams.

combined  $\pi$  and  $K$  beam distributions are found to be consistent with one another. Therefore, in order to minimize systematic errors due to uncertainty in the measured  $x_F$  and  $p_T^2$  distributions (see Section 8.2 for the sizes of these errors), combined  $D$  cross-sections (for combined  $\pi$ , combined  $K$ , or  $p$  beams) are used to weight all pseudoscalar  $D$  MC events.  $D^{*+}$  measured distributions for combined  $\pi$  and  $p$  beams are used to weight this species' MC.<sup>7</sup>

<sup>7</sup>For  $D^{*+}$ , the combined  $K$  beam measurements are not measured with enough precision to justify

MC events are weighted by the following functions:

$$F_{prod.dist.}(x_F, p_T^2) = \frac{N_{meas}(x_F)}{N_{gen}(x_F)} \frac{M_{meas}(p_T^2)}{M_{gen}(p_T^2)}, \quad (7.3)$$

where the subscript “*meas*” denotes a function proportional to the relevant differential cross-section and “*gen*” denotes a functional fit to the number of MC-generated events as a function of the relevant production variable. So that no weighting of generated events is necessary, the numerator functions are normalized so that their areas ( $x_F > 0$ ) are equal to the areas of the denominator functions (i.e., equal to the total number of MC events generated in the forward hemisphere).

Typical MC-generated distributions are shown in Fig. 7.3. For all species, the generated distributions in  $x_F$  were fit by the form given in Equation 2.7, in  $p_T^2$  by that given in Equation 2.10. Data distributions in  $x_F$  are fit using the same composite function used for the MC. Versus  $p_T^2$ , however, combined  $K$  and  $p$  beam distributions are fit to a simple exponential (see Equation 9.11), while the combined  $\pi$  beam distribution is fit with the two-component FMNR form used for the MC.

As described in Section 4.1, the MC event generator uses  $\pi$ -nucleon collisions as the starting point for every simulated event. We therefore expect the weighting correction described in this section to be largest for  $p$  beam, especially versus  $x_F$ . In Figs. 7.4 and 7.5, the weighting correction functions used for  $D^+$  MC are shown. In regions where significant fractions of the events reside, the weighting is fairly slight. In order to judge the effect of the weighting on the acceptance, however, we must also convolve these weightings with the variation of the differential acceptances in the important  $x_F$  and  $p_T^2$  ranges (see Section 7.4). Not surprisingly, the impact on acceptance of these corrections to the MC production distributions is small; for example, the largest of the  $D^+$  acceptance relative shifts ( $p$  beam) is only about 4%.

---

using them to weight the MC; all meson beam-induced distributions are taken to be consistent with the  $\pi$  beam result.

### 7.2.4 Lifetime distributions

The proper lifetime  $t$  of a charm particle is strongly correlated to the significance of  $z$ -separation between primary and secondary (i.e., production and decay) vertices. Since a cut on SDZ is an essential component of event selection for each charm decay mode in this analysis, we expect the acceptance to depend significantly on the lifetime distributions of the various charm species. Therefore, it is crucial that the average lifetimes assumed by the MC generator agree with the best measurements available. As can be seen from Table 7.2, this agreement is quite good for the pseudoscalar mesons in question.

Particle	lifetime $\tau$ (ps)	
	Lund	1994 PDG
$D^+$	1.069	$1.057 \pm 0.015$
$D^0$	0.428	$0.415 \pm 0.004$
$D_s$	0.436	$0.467 \pm 0.017$

Table 7.2: MC and world average lifetime values.

In the absolute cross-section analysis, MC events are weighted as a function of their proper lifetime in order to correct for the small discrepancies between the 94 PDG and Lund truth table lifetimes. The weighting function takes the following form:

$$F_{\tau dist.}(t) = \frac{\tau_{Lund}}{\tau_{PDG}} \frac{\exp -t/\tau_{PDG}}{\exp -t/\tau_{Lund}}, \quad (7.4)$$

where the normalization factor gives the two exponential distributions the same area, making weighting of generated events unnecessary, as with the production distribution correction. The relative shifts in the acceptances due to this lifetime distribution weighting are on the order of (but less than) the relative shifts in the lifetimes themselves; this correction brings about relative shifts in the acceptances from  $\sim 1\%$  for  $D^+$  to  $\sim 3\%$  for  $D_s$ .

### 7.2.5 Drift chamber efficiency

As described in Section 4.2, the average efficiencies of two drift chamber planes (D12,  $u$  and  $v$  views) were not adequately matched by the input efficiencies used in the positive digitizer. A corrected version of the digitizer, using modified average efficiencies for these two drift chambers, was implemented for  $D^+$  and  $D^0$  modes;  $D_s$  MC events, however, were digitized using the old default plane efficiencies.

Run region	beam	$\chi_{DC}$
3	$\pi^+$	1.038
	$K^+$	1.046
	$p$	1.030
4	$p$	0.884

Table 7.3: Positive running DC correction factors.

The new D12 $u$  and D12 $v$  input efficiencies were chosen to match output efficiencies (as returned by the reconstruction code) equaling flux-weighted averages of the measured efficiencies of these two planes (obtained as a function of run number from a sample of PASS0 tapes). These planes were inoperative for significant portions of the positive running (see Section 4.2 for a detailed history). Due to the large fluctuations in these efficiencies, acceptances obtained using positive-digitized MC do not reflect the average efficiencies of the two DC planes in question for run regions corresponding to data subsets (i.e., Regions 3 and 4). Therefore, correction factors were calculated for Regions 3 and 4 using the appropriate flux-weighted averages of acceptances obtained with  $D^+$  MC events digitized to model *separately* the three important regions characterizing D12 $u$  and D12 $v$  performance (the so-called “on/on”, “off/off”, and “on/off” regions). These multiplication factors  $\chi_{DC}$  are calculated as follows:

$$\chi_{DC}(\text{Region } x) = \frac{\sum_i f_i^x \text{Acc}_i}{\text{Acc}_{def}}, \quad (7.5)$$

where the summation runs over the three DC performance regions, the weighting

factors  $f_i^x$  give region  $i$ 's flux fraction in Region  $x$ ,  $Acc_i$  is the  $D^+$  acceptance in region  $i$ , and  $Acc_{def}$  is the  $D^+$  acceptance averaged over the positive running.

Since differential distribution and trigger efficiency weightings are dependent upon the data subset being simulated,  $\chi_{DC}$  is calculated separately for each beam particle appropriate to a particular run region; these values are given in Table 7.3. The systematic errors associated with these correction factors are discussed in Section 8.2.

### 7.2.6 Data subset combination

In the differential analysis, acceptance distributions versus  $x_F$  and  $p_T^2$  are needed for combinations of two or more data samples (e.g., two particles or two beams) when the signal estimates for these joint samples are obtained by a fit to a single histogram. In these cases, the corresponding MC signals are combined into a joint histogram as well. As with the data (see Section 6.3), an explicit mass shift is introduced so that different particles can be fit under a single Gaussian. The MC is weighted, however, so that the relative amounts of each constituent event type within the MC signal will mirror the data. Depending on the data sets that are being combined, this weighting can be a function of relative cross-section, branching fraction ( $B$ )<sup>8</sup>, prescaler value, flux, or number of MC events generated. In combining  $D^+$ ,  $D^0$ , and  $D_s$  mesons into combined  $D$  signals, the ratios of the cross-sections are assumed to be 2:4:1. Below are given calculations of the various weighting factors  $w(x)$ , where  $x$  indicates the type of MC events actually weighted in a particular combination scenario:

Combining beam particles:

$$\begin{aligned} w(\pi^+ \text{ beam}) &= \left( \frac{\pi^+}{\pi^-} \right)_{data} \\ &= \left( \frac{1.0481 \times 10^{11}}{7.0086 \times 10^{10}} \right)_{flux} \times \left( \frac{.18081}{.30794} \right)_{prescaler} = 0.879 \end{aligned} \quad (7.6)$$

$$\begin{aligned} w(K^- \text{ beam}) &= \left( \frac{K^-}{K^+} \right)_{data} \\ &= \left( \frac{2.2570 \times 10^9}{5.5848 \times 10^9} \right)_{flux} = 0.404 \end{aligned} \quad (7.7)$$

---

<sup>8</sup>We label branching fractions of charm species and their unstable decay products  $B_{primary}$  and  $B_{secondary}$ , respectively.

Combining decay modes:

$$\begin{aligned}
\left(\frac{D_s \rightarrow K^* K}{D_s \rightarrow \phi \pi}\right)_{data} &= \left(\frac{3.3\%}{3.5\%}\right)_{Bprimary} \times \left(\frac{66.7\%}{49.1\%}\right)_{Bsecondary} = 1.281 \\
\left(\frac{D_s \rightarrow K^* K}{D_s \rightarrow \phi \pi}\right)_{MC} &= \left(\frac{66.7\%}{49.5\%}\right)_{Bsecondary} \times \left(\frac{200K}{150K}\right)_{\#generated} = 1.796 \\
w(D_s \rightarrow K^* K) &= \left(\frac{D_s \rightarrow K^* K}{D_s \rightarrow \phi \pi}\right)_{data} \times \left(\frac{D_s \rightarrow \phi \pi}{D_s \rightarrow K^* K}\right)_{MC} \\
&= \frac{1.281}{1.796} = 0.713
\end{aligned} \tag{7.8}$$

Combining particles:

$$\begin{aligned}
w(D_0 \rightarrow K\pi) &= \left(\frac{D^0 \rightarrow K\pi}{D^+ \rightarrow K\pi\pi}\right)_{data} \\
&= \left(\frac{2}{1}\right)_{cross-section} \times \left(\frac{4.01\%}{9.1\%}\right)_B = 0.881 \\
\left(\frac{D_s \rightarrow \phi\pi}{D^+ \rightarrow K\pi\pi}\right)_{data} &= \left(\frac{1}{2}\right)_{cross-section} \times \left(\frac{3.5\% \times 49.1\%}{9.1\%}\right)_B = 0.094 \\
\left(\frac{D_s \rightarrow \phi\pi}{D^+ \rightarrow K\pi\pi}\right)_{MC} &= \left(\frac{49.1\%}{100\%}\right)_{Bsecondary} = 0.491 \\
w(D_s \rightarrow \phi\pi) &= \left(\frac{D_s \rightarrow \phi\pi}{D^+ \rightarrow K\pi\pi}\right)_{data} \times \left(\frac{D^+ \rightarrow K\pi\pi}{D_s \rightarrow \phi\pi}\right)_{MC} \\
&= \frac{0.094}{0.491} = 0.191
\end{aligned} \tag{7.10}$$

### 7.3 MC signals

MC signals are fit (also using log-likelihood) with the same function used to fit the data, except that only flat backgrounds are used. Mass and width are allowed to float. Incidentally, the quality of these fits (as indicated by  $\chi^2/dof$  and confidence level<sup>9</sup>) is quite low for high-statistics signals. The returned signal estimates, nevertheless, are accurate (deviations on the order of  $1\sigma$ ) estimators of the number of MC signal events.

As in the data signal fits, the fitting procedure is modified for signals binned in  $x_F$  and  $p_T^2$ ), as described in Sections 7.3.1 and 7.3.2. The widths and masses returned

---

<sup>9</sup>When the term ‘‘confidence level’’ is used with regard to fit quality, it refers to the  $\chi^2$  upper-tail probability.

by fits of the total negative (see later comments) MC signals are listed in Table 7.4.

Decay mode	width (MeV)	mass (MeV)
$D^+ \rightarrow K\pi\pi$	$9.38 \pm 0.10$	$1870.5 \pm 0.1$
$D^0 \rightarrow K\pi$	$10.41 \pm 0.12$	$1866.4 \pm 0.1$
$D^* \rightarrow D^0\pi$	$11.1 \pm 0.2$	$2012.1 \pm 0.2$
$D_s \rightarrow KK\pi$	$8.18 \pm 0.13$	$1970.6 \pm 0.1$
Combined $D$	$9.74 \pm 0.07$	$1870.7 \pm 0.1$

Table 7.4: MC signal widths and masses.

For  $D^+ \rightarrow K\pi\pi$ , the negative and positive MC signals are found to have the same width and mass within statistics; for  $D^0 \rightarrow K\pi$ , the differences in width and mass are marginally significant but less than 1 MeV. Therefore, for purposes of this analysis, negative and positive MC are assumed to have the same width and mass. (This becomes relevant soon.) A sampling of fitted MC signals are shown in Fig. 7.6.

### 7.3.1 MC signals vs. $x_F$

Signal width is known to be a function of  $x_F$ ; this dependence is obtained from the MC by fitting signals in 0.1 bins of  $x_F$ . In order to minimize the effects of low statistics, the mass of the MC signals is fixed to the mass obtained from the fit of the total MC signal (typically about 1 MeV higher than the 94 PDG mass value). The significance of the  $x_F$ -binned MC signals begins to peter out rapidly after the 0.5-0.6 bin; as a result, the widths obtained in the higher- $x_F$  fits fluctuate wildly, both high and low. Therefore, the widths obtained in the  $x_F$  range -0.1-0.6 are fitted with a third-order polynomial in order to obtain a smooth function of signal width versus  $x_F$ . Widths beyond  $x_F$  of 0.6 are determined by projecting this function linearly, using the width and slope at  $x_F$  of 0.5. These functions are displayed along with MC signal widths versus  $x_F$  in Fig. 7.7. Due to limited statistics, the MC signal widths for the modes  $D^* \rightarrow D^0\pi$  and  $D_s \rightarrow KK\pi$  are fixed using the width functions obtained

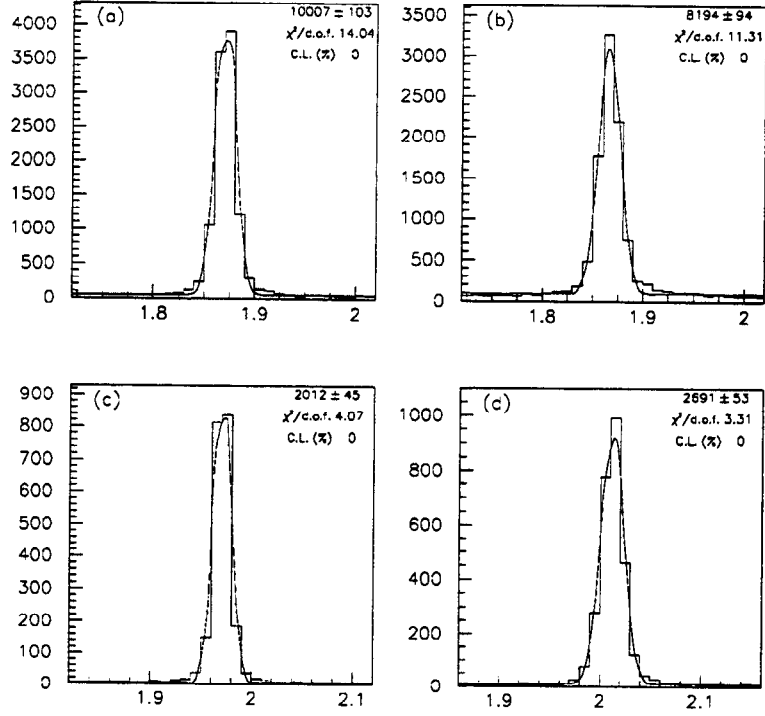


Figure 7.6: Negative-digitized unweighted MC events vs. invariant mass (GeV),  $x_F > 0$ , for (a)  $D^+ \rightarrow K\pi\pi$ , (b)  $D^0 \rightarrow K\pi$ , (c)  $D_s \rightarrow \phi\pi$ , and (d)  $D^* \rightarrow D^0\pi$ .

from  $D^0 \rightarrow K\pi$  and  $D^+ \rightarrow K\pi\pi$  MC respectively (offset by amounts indicated by the total MC signals).

The legitimacy of fixing the MC signal mass to a constant value in all bins of  $x_F$  was examined by refitting the  $D^+ \rightarrow K\pi\pi$  MC signals, allowing the mass to float while keeping the widths fixed. Although some systematic dependence of the signal mass on  $x_F$  is apparent (see Fig. 7.8), deviations from constant mass are on the order of a few MeV in the  $x_F$  range of most interest. Fixing the mass at values 2 MeV greater and lower than that used in the analysis has no significant impact on the signal estimates returned by the fitter.

In order to determine the signals that go into the calculation of acceptance versus  $x_F$ , the MC signals are *refit*, this time fixing the mass *as well as* the widths (using the smooth signal width function). It should be noted that it is the negative MC that is

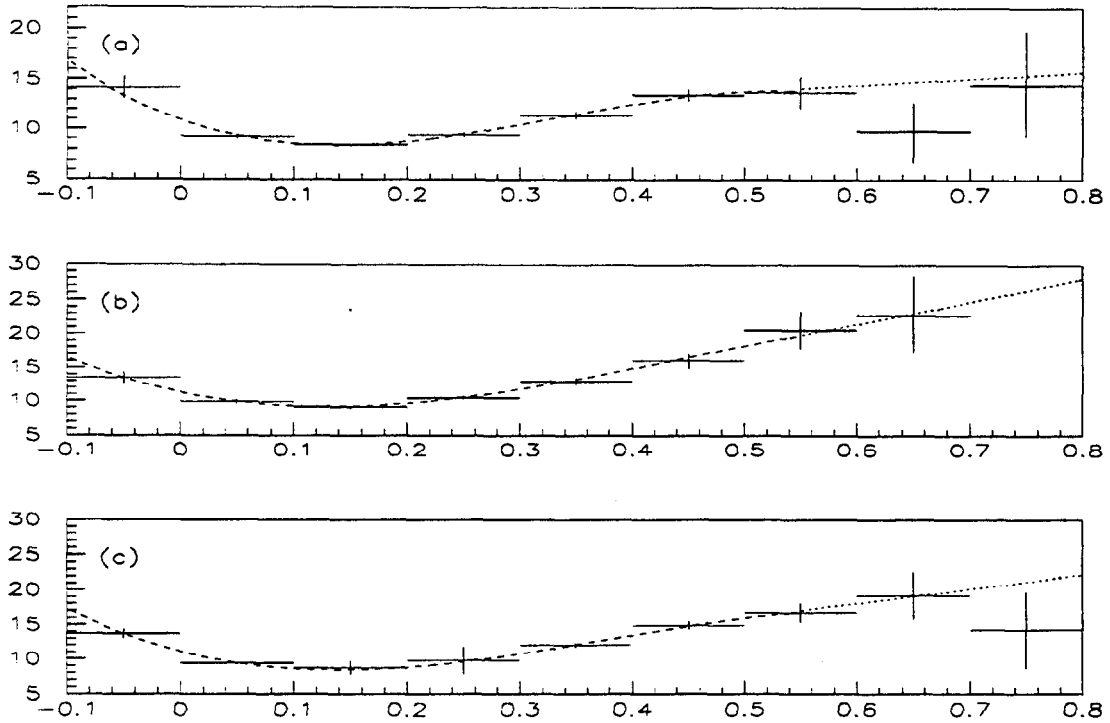


Figure 7.7: MC signal width (MeV) vs.  $x_F$  for (a)  $D^+ \rightarrow K\pi\pi$ , (b)  $D^0 \rightarrow K\pi$ , and (c) combined  $D$ .

used to obtain the signal widths. For  $D^+ \rightarrow K\pi\pi$ , the negative and positive MC are found to give signal width functions with consistent parameters. For  $D^0 \rightarrow K\pi$ , the correspondence is not as close. Nevertheless, for this mode the positive MC signal estimates obtained using the negative MC signal width function are completely consistent with those obtained using the positive MC signal width function. Therefore, for the sake of simplicity, the negative MC width functions are used across the board. Examples of these fits and the resulting signal estimates are shown for the unweighted negative-digitized combined  $D$  MC signals in Fig. 7.9.

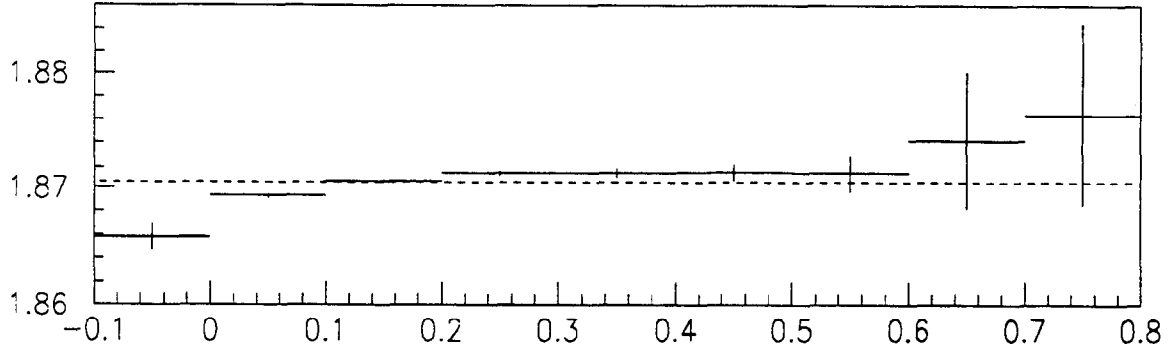


Figure 7.8:  $D^+ \rightarrow K\pi\pi$ , negative MC, signal mass (GeV) vs.  $x_F$ . The dotted line indicates the constant mass value used in the  $D^+ \rightarrow K\pi\pi$  analysis.

### 7.3.2 MC signals vs. $p_T^2$

In fitting MC signals broken down into bins of  $p_T^2$  (see Section 6.3.2 for a discussion of the variable binwidths used in the  $p_T^2$  analysis), it is assumed that the signal width does not vary as a function of  $p_T^2$ . Both mass and width are fixed to the values obtained from the fit of the total MC signal.

Fits and signal estimates are shown for unweighted negative-digitized combined  $D$  modes MC signals in Fig. 7.10. Note that the entire  $p_T^2$  analysis is carried out using positive  $x_F$  signals (MC and data) only. Where units are not explicitly shown,  $p_T^2$  is measured in  $\text{GeV}^2$ .

## 7.4 Results

In Table 7.5, “geometric” efficiencies  $\epsilon_{geom}$  are shown for each decay mode. Values are shown for  $\pi^-$  and  $\pi^+$  beams in order to show the variation of this efficiency with running conditions (the most important of which is beam intensity). As described in Section 7.2.3, dependence of  $\epsilon_{geom}$  on beam particle type is relatively weak, so kaon and proton beam values are not tabulated. Note, however, that a significant fraction of the  $p$ -induced signal events were produced in Region 4, during which  $\epsilon_{geom}$  is about

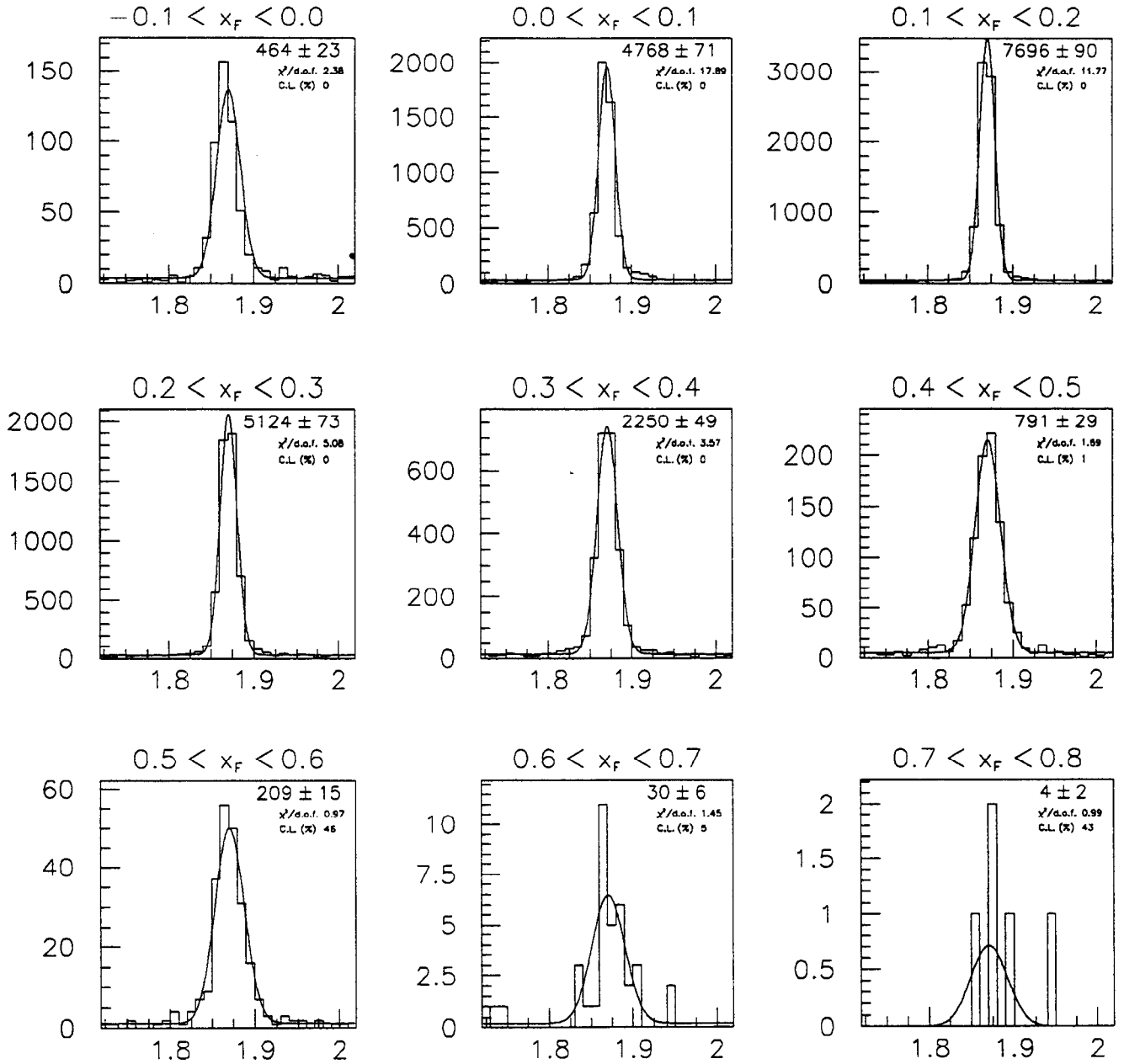


Figure 7.9: Combined  $D$  unweighted negative-digitized MC events vs. invariant mass (GeV).

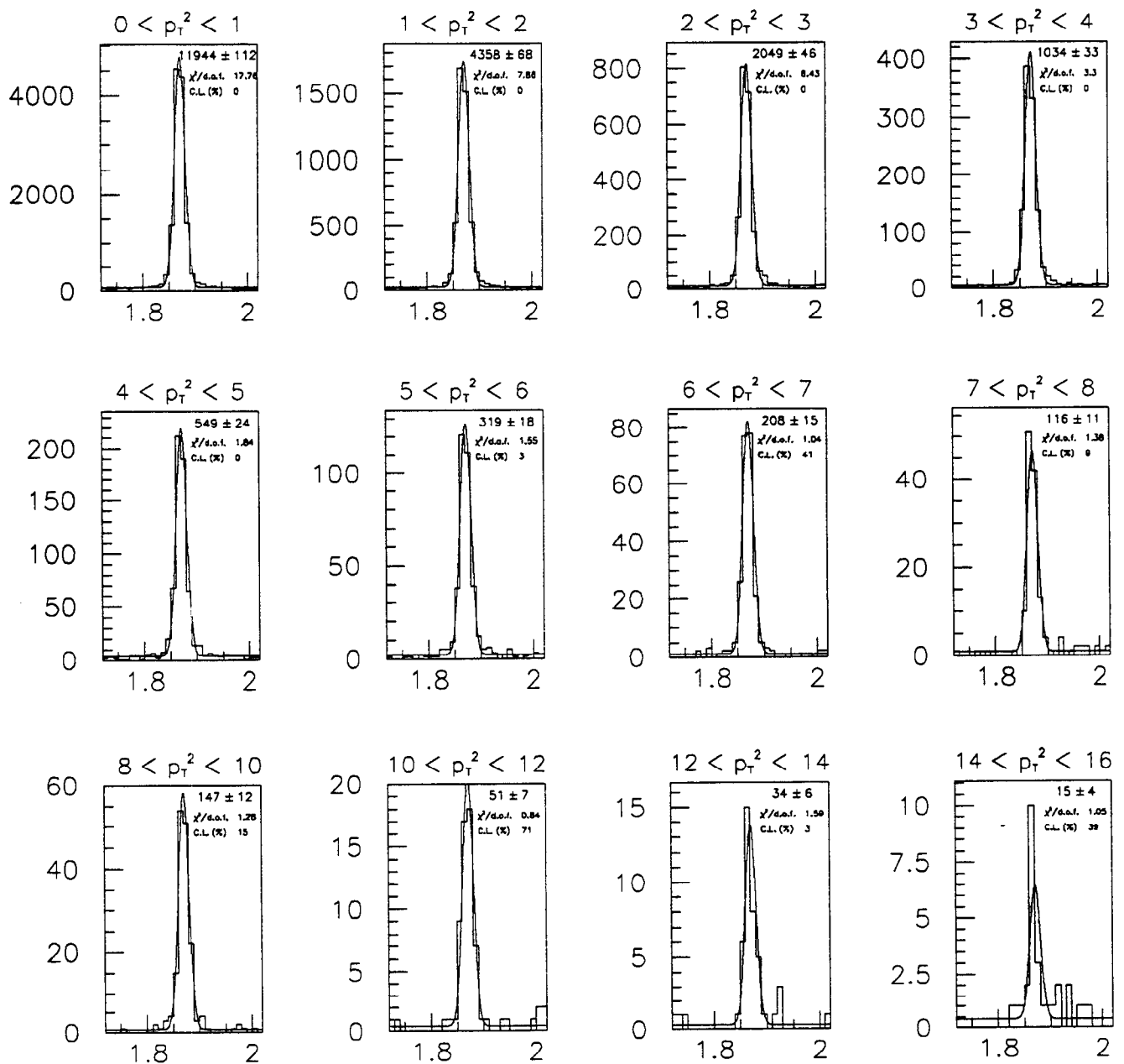


Figure 7.10: Combined  $D$  unweighted negative-digitized MC events vs. invariant mass (GeV),  $x_F > 0$ .

17% lower than in Region 3 due to drift chamber conditions (see Section 7.2.5).

Decay mode	$\epsilon_{geom}(B = \pi^-)$ (%)	$\epsilon_{geom}(B = \pi^+)$ (%)
$D^+ \rightarrow K\pi\pi$	$8.35 \pm 0.08$	$5.93 \pm 0.07$
$D^0 \rightarrow K\pi$	$6.85 \pm 0.08$	$5.36 \pm 0.07$
$D^* \rightarrow D^0\pi$	$7.75 \pm 0.15$	$5.59 \pm 0.13$
$D_s \rightarrow \phi\pi$	$3.47 \pm 0.08$	$2.31 \pm 0.06$
$D_s \rightarrow K^*K$	$2.29 \pm 0.05$	$1.49 \pm 0.04$

Table 7.5: “Geometric” efficiencies, ( $x_F > 0$ ).

The errors on  $\epsilon_{geom}$  are determined by taking the *relative* errors on efficiencies derived from weighted and unweighted MC events to be equal; the absolute error on the latter is simply the error on the binomial probability  $\epsilon$ :

$$\sigma_\epsilon = \sqrt{\frac{(1-\epsilon)\epsilon}{N_{gen}^{MC}}}, \quad (7.11)$$

where  $\epsilon$  in this case is the “raw” efficiency calculated with unweighted MC. In the rest of this chapter, errors shown on acceptances will be those derived from MC statistics as just described. Additional systematic errors arising from the various weightings used (e.g.,  $\epsilon_{trig}$ ) are detailed in Section 8.2.

As defined in the first section of this chapter, “acceptance” is the product of efficiencies  $\epsilon_{trig}$  and  $\epsilon_{geom}$ , where the former includes the effect of prescaling. Trigger efficiencies and forward acceptances for  $D^+ \rightarrow K\pi\pi$  are given in Table 7.6. Because  $\epsilon_{trig}$  is only weakly dependent on the identities of the charm species in the event, information from Tables 7.5 and 7.6 is sufficient to obtain estimates of acceptance for any data subset/charm meson decay combination relevant to this analysis. The errors shown for the tabulated acceptances arise from MC statistics only; systematic errors in acceptance (including those associated with  $\epsilon_{trig}$ ) are detailed in Section 8.2.2.

The shapes of the differential acceptances do not depend strongly on either charm

Data subset <sup>a</sup>	$\epsilon_{trig}(T, D^+ \rightarrow K\pi\pi)^b$ (%)	$Acc(D^+ \rightarrow K\pi\pi)$ (%)
Reg. 1 $\pi^-$	38	$3.18 \pm 0.03$
Reg. 2 $\pi^-$	17	$1.406 \pm 0.013$
Reg. 1 $K^-$	78	$6.51 \pm 0.06$
Reg. 2 $K^-$	78	$6.41 \pm 0.06$
$\pi^+$	6	$0.355 \pm 0.004$
$K^+$	89	$5.27 \pm 0.06$
$p$	9	$0.513 \pm 0.006$

<sup>a</sup>In most cases, specification of the beam particle type is sufficient to determine the data subset (listed in Section 6.2). It must be kept in mind, however, that these data subsets are in general *also* distinguished by different trigger types and run regions.

<sup>b</sup>Recall that these trigger efficiencies include the effects of prescalers.

Table 7.6:  $D^+ \rightarrow K\pi\pi$  trigger efficiencies and acceptances, ( $x_F > 0$ ).

species or data subset. To support the former independence, combined  $\pi$  beam acceptances are shown for each charm meson species versus  $x_F$  and  $p_T^2$  in Figs. 7.11 and 7.12, respectively. The latter is supported by Figs. 7.13 and 7.14, in which combined  $D$  acceptances are shown for different beams versus  $x_F$  and  $p_T^2$ , respectively. The absolute scales of these acceptance plots are correct, given that inefficiencies due to prescalers are not included.<sup>10</sup>

In the combined  $D$  acceptance plots, the combined  $K$  beam subset has the highest acceptance because all of the data is required to pass only the low- $E_T$  threshold. Next comes the combined  $\pi$  beam subset, the acceptance of which is lowered by the effect of the relative  $\pi^-/\pi^+$  prescale and the presence of a component coming in under the high- $E_T$  threshold. Finally, the  $p$  beam subset has the lowest acceptance, due not only to a high- $E_T$  component but also to a Region 4 component, with its reduced drift chamber efficiency.

<sup>10</sup>In the case of combined  $\pi$  and  $p$  beam acceptances, where two data subsets with differing average prescalers are averaged, the MC is normalized so that the effect of the prescaler on the *more populated* subset is removed; a relative prescale between the two subsets remains.

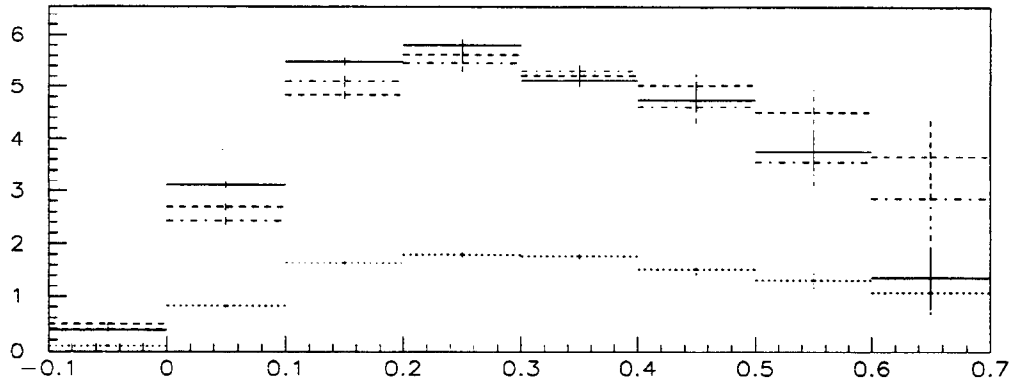


Figure 7.11:  $\pi$  beam acceptance (%) vs.  $x_F$  for  $D^+ \rightarrow K\pi\pi$  (solid),  $D^0 \rightarrow K\pi$  (dashed),  $D_s \rightarrow KK\pi$  (dotted), and  $D^* \rightarrow D^0\pi$  (dot-dashed).

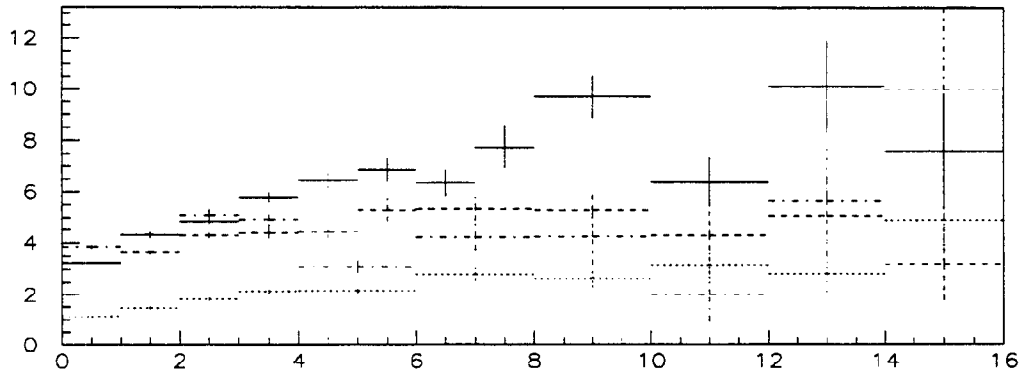


Figure 7.12:  $\pi$  beam acceptance (%) vs.  $p_T^2$  ( $\text{GeV}^2$ ) for  $D^+ \rightarrow K\pi\pi$  (solid),  $D^0 \rightarrow K\pi$  (dashed),  $D_s \rightarrow KK\pi$  (dotted), and  $D^* \rightarrow D^0\pi$  (dot-dashed).

As detailed earlier, weighting is introduced when combining MC signals in order to force the relative fractions of each constituent to match those in the corresponding combined data signals. This weighting (except for that simulating relative prescaler values) must also be used to obtain the correct total number of generated MC events. The ratio of these quantities gives the acceptance for combined samples. The error on this acceptance, however, cannot be obtained by simply evaluating the binomial error on the “raw” acceptance, as that would give each constituent equal statistical power

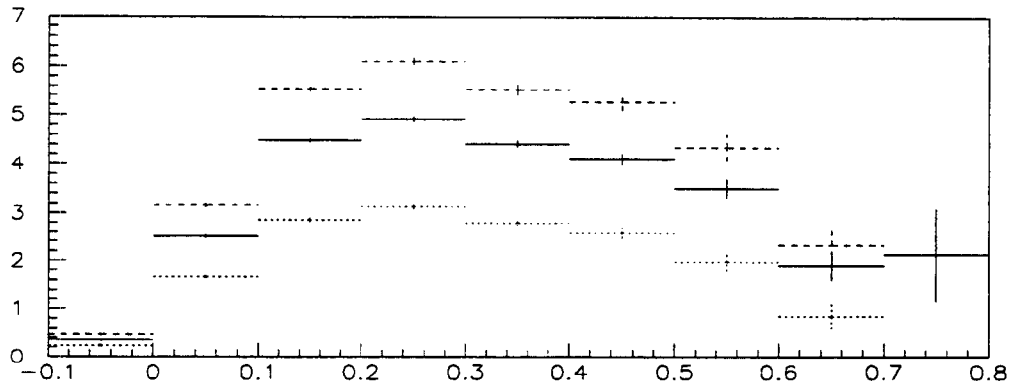


Figure 7.13: Combined  $D$  acceptance (%) vs.  $x_F$  for combined  $\pi$  beam (solid), combined  $K$  beam (dashed), and  $p$  beam (dotted).

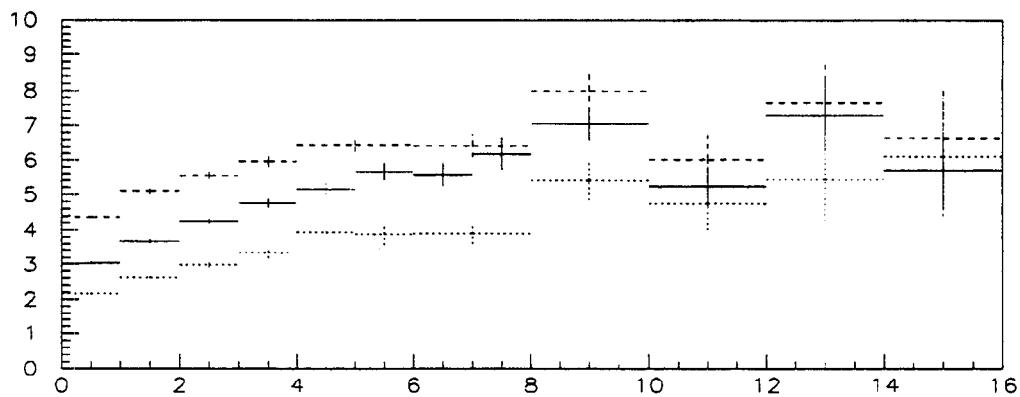


Figure 7.14: Combined  $D$  acceptance (%) vs.  $p_T^2$  ( $\text{GeV}^2$ ) for combined  $\pi$  beam (solid), combined  $K$  beam (dashed), and  $p$  beam (dotted).

(assuming an equal number of generated events) despite the fact that some comprise only a small fraction of the signal after weighting. Therefore, the relative error of a “combined” acceptance is taken to be equal to that of the fraction-weighted sum of the constituent acceptances, each of whose relative errors are in turn derived from their “raw” acceptances, as described above. The combined  $D$  calculation is given as an example:

$$\frac{\sigma(Acc_D)}{Acc_D} = \frac{\sigma(\sum_i wgt_i Acc_i)}{\sum_i wgt_i Acc_i} = \frac{\sqrt{\sum_i (wgt_i \sigma(Acc_i))^2}}{\sum_i wgt_i Acc_i}, \quad i = \begin{cases} D^+ \\ D^0 \\ D_s \rightarrow \phi\pi \\ D_s \rightarrow K^* K \end{cases} \quad (7.12)$$